•土木工程•

DOI:10.12454/j.jsuese.202300583

本刊网刊

基于有源波导系统土体剪切试验过程声发射特征演化规律

吴　鑫[1,2],刘永红[1],王雪梅[1,3],张　满[1]

(1.四川师范大学 工学院,四川 成都 610101;2.四川师范大学 西南土地资源评价与监测教育部重点实验室,四川 成都 610068;
3.眉山市应急管理局,四川 眉山 620020)

摘　要:近年来,土质边坡稳定性监测技术获得了较大发展,但滑坡体内部剪切过程监测和潜在风险感知仍然存在不少困难。本文利用有源波导系统和声发射(acoustic emission)技术研究土体在不同剪切条件下的AE信号特征演化规律。研究表明:振铃计数随剪切位移增加而迅速增大,并随含水率的增加呈幂函数减小;能量随着剪切位移加大呈现缓慢增加趋势,且含水率低、加载速率快的土样释放声发射能量更大;b值(岩土体破坏过程中AE小事件数与大事件数的比)随剪切位移先降低后平缓,宏观破坏发生后b值逐步稳定,而含水率与其成负相关。此外,试验揭示了AE信号的多因素演化规律,在振铃计数–b值空间中,随含水率的降低特征向量逐次向右下方移动,即低含水率试样总是具有更低的b值和更大的振铃计数;在振铃计数–能量空间中,随含水率增加,结果分布逐次向右上角移动,即能量和振铃计数同时增大;加载速率对结果分布形态亦有一定影响,且剪切速率越大,类间分离度越高。研究成果可为声发射技术在土质边坡滑动预测预警中特征指标选取提供理论依据。

关键词:土体剪切;加载速率;含水率;声发射;特征参数

中图分类号:TU4　　**文献标志码**:A　　**文章编号**:2096-3246(2025)03-0096-10

随着中国基础设施建设的迅速发展,工程施工造成的自然环境人工扰动逐渐增加,各类地质灾害形势日趋严峻,其中,滑坡灾害对工程建设和生命财产安全造成了很大威胁[1–4]。近年来,除常规的位移、应力、地下水及降雨量监测等,许多新技术也被运用于边坡稳定性监测,如测斜仪、阵列式位移计(SAA)等新型传感器,以及3D扫描仪、GPS、GIS、RS及干涉合成孔径雷达等[5]。这些技术主要是利用地表或一定深度范围的位移和变形场进行边坡稳定性预测,因此属于基于“变形趋势”的预测方法。这类方法具有逻辑清楚、结果较为准确的特点,但只有当边坡已出现滑移或变形时才能确定其状态变化,无法捕捉到土体内部正在发生的剪切破坏过程及破坏强度等实时信息。由于岩土体边坡破坏过程总是伴随着微裂缝的萌生、发育和扩展,该过程会以各类弹性波的形式释放能量[6–8],即声发射现象。Shiotani[9]对比了土质边坡失稳中微震与声发射之间的差异,发现前期预测可使用较高共振频率的AE传感器,而频率较低的微震传感器则对后期较敏感。Dixon等[10]将声发射用于检测土壤颗粒间摩擦和位移。李刚[11]和李文彪[12]等将声发射用于松散颗粒介质边坡或路堤稳定性研究。Codeglia等[13]开发了一种利用波导杆从剪切区域向传感器传输AE信号的系统,采用振铃计数(RDC)量化声发射活动并在现场长期监测,得到AE信号与地下水位及积雪等之间的关系。Jiang等[14]开展了多种情况下的颗粒材料环剪试验,发现剪切阻力、压实度和滑移位移及声能释放与剪切速率和粒径的关联,并证实基于AE的破坏先兆预测的可行性。Hu等[15]提出用声发射和微震联合监测,获得更准确和及时的预测结果。Berg等[16]利用声发射开展极慢型(小于15 mm/a)路基边坡深层滑动监测,成功检测到约5 mm/a的极慢滑动速度,证明了声发射对位移速率变化非常敏感。

以上研究成果说明,利用声发射技术对岩土体边坡失稳进行监测或预测是可行的。为进一步分析土体物理力学参数对剪切破坏过程中声发射特征演化规律的影响机制,比较土质边坡预测的特征参数敏感

收稿日期:2023 – 07 – 30　　**修回日期**:2024 – 07 – 05　　**网络出版日期**:2024 – 09 – 30

基金项目:中华人民共和国应急管理部安全生产重特大事故防治关键技术项目(Sichuan–0011–2018AQ);四川省科技计划项目(24NSFSC0343;19YYJC2854)

作者简介:吴　鑫(1983—),男,副教授.研究方向:矿山岩土力学与灾害防治.E-mail:xinwu@sicnu.edu.cn

性及规律性，拟以加载速率和土体含水率为变量，开展土体双面剪切破坏过程中声发射特征演化规律研究。相关成果可为建立声发射监测预警系统及其指标选取提供理论支持。

1　试　验

1.1　试验装置及材料制备

试验系统主要由土体剪切系统和DS5–16B型声发射数据采集系统组成，如图1所示。图1中，d为填充砂粒的粒径。声发射主机采样频率为3 MHz，采用增益为40 dB的前置放大器、型号为RS–2A的陶瓷压电传感器（频率响应范围为100~400 kHz），以硅凝胶为耦合剂，采用电子万能材料试验机位移控制式加载，压头作用于中间段剪切盒，形成竖向双剪切面。由于声发射信号在土体等颗粒堆积物中传播时衰减速度较快[17–18]，因此，采用有源波导杆（active waveguide）的形式监测[19–25]，即通过波导杆周围回填颗粒材料的摩擦挤压产生和放大AE信号，然后通过波导杆导出，提高数据监测的灵敏度并降低衰减[26]。试验采用直径为20 mm、长度为500 mm的Q235型实心圆钢为波导杆；采用直径为1~2 mm的筛选砂粒为填充材料；采用3个长、宽和高均为150 mm的不锈钢铁盒为模拟剪切装置，剪切盒中心孔直径为40 mm。

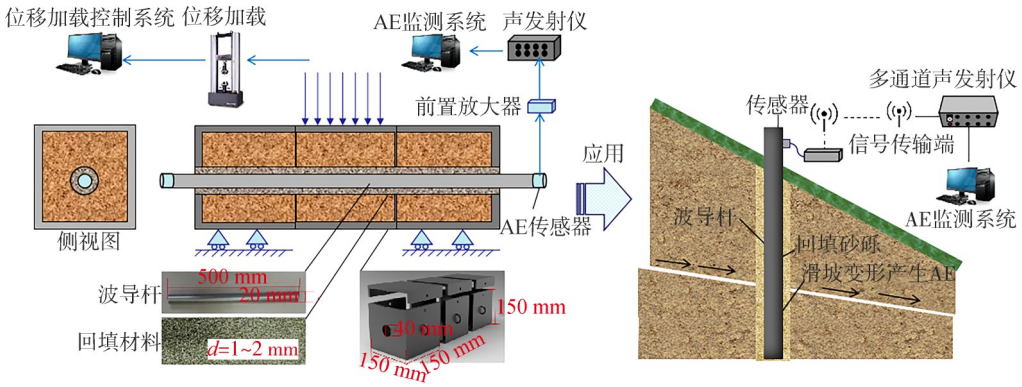

图1　土体剪切试验声发射监测系统

Fig. 1　Acoustic emission monitoring system for soil shear test

试样装填及试验过程如图2所示。首先，采用成都市东郊和新都区以南分布广泛的黏土作为试验材料，其为分布在岷江三级阶地上的沉积物，具有高含水量、丰富的黏土组分、复杂的孔隙结构，去除土体中所含较大结核块体等杂质；其次，用黏土逐层装填并压实至剪切盒中心孔高度（图2(a)）；接着，在土体中央位置开槽，铺设填充材料，确保波导杆放置于回填材料中间，两端刚好能穿过预留中心孔，避免与剪切盒接触，注意填充材料应均匀且完全包裹波导杆（图2(b)、(c)）；再次，将黏土表面刮毛后，逐层填充并压实至装满整个剪切盒，合上盒盖，拧好剪切盒侧面的螺丝固定装置，防止剪切过程中土体发生横向膨胀变形，将剪切装置放置于材料试验机上（图2(d)）；然后，清理剪切盒上覆盖的多余黏土，在波导杆两端涂上耦合剂，用橡皮筋将声发射传感器固定在其两端（图2(e)）；最后，通过位移控制式加载，加载至剪切破坏，达到预定位移后停机，记录全过程AE信号和加载数据并进行分析（图2(f)、(g)）。

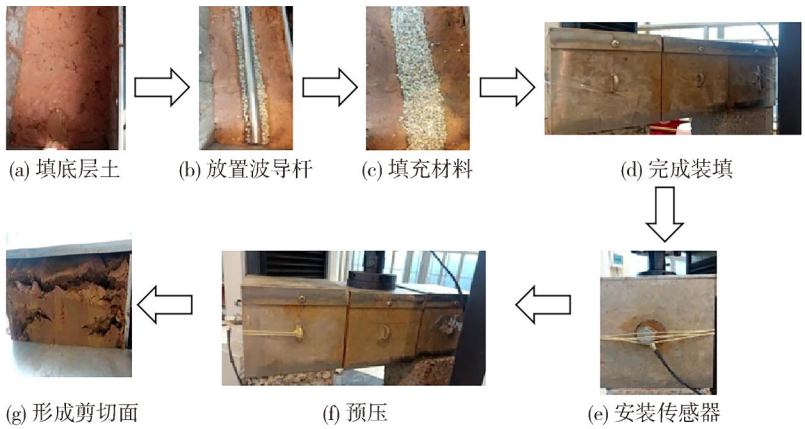

图2　试样装填及试验过程

Fig. 2　Sample loading and testing process

1.2 试验过程

为探究土体剪切过程中声发射信号与加载速率及含水率之间的内在联系，分别以二者为变量设计试验，加载速率共计3组，分别为5、10、20 mm/min；每组加载速率下设5种不同的含水率，共计15组试验。试验开始前，电子万能材料试验机先以5 mm/min的加载速率对土体进行预压测试，预压力可减少盒盖与土体等之间的空隙，预压力一般设置为0.2 kN。试验剪切总位移设置为50 mm，达到后立即停机，然后重新装填进行下一组剪切试验。然后，将土体放置24 h，等待水分自然蒸发。24 h后继续重复上述3组不同加载速率下的剪切试验，以此类推，完成15组试验。每次试验用黏土质量均在19.52~19.66 kg之间，每次试验结束后取30 g黏土按土工试验方法标准（GB/T 50123—2019）留样并测定其准确含水率。

2 AE特征参数分析

2.1 土体剪切试验结果

采用位移控制式加载，设置停机终止位移为50 mm，由于总加载位移相同，加载速率分别为5、10、20 mm/min，对应加载时间分别为600、300、150 s。黏土剪切试验方案与结果如表1所示。图3为土体在不同加载速率下含水率与剪切力关系曲线。以图3（a）为例：含水率为19.0%、20.5%、21.0%、22.0%、23.5%时，发生剪切破坏的力分别约为2.12、1.37、1.17、0.92、0.80 kN；随着含水率的增加，破坏土体所需的抗力降低。其余两个试验结果类似。其原因在于，当含水量增加时，吸附在颗粒周围的水膜加厚，土粒周围强结合水外侧形成了弱结合水，强结合水性质接近固态，而弱结合水呈黏滞状态，受力时可变形或滑动。因此，含水量增加将导致黏土内聚力下降，从而导致土质变软、承载力变差。

表1 黏土剪切试验方案与结果

Tab. 1 Clay shear test plan and results

加载速率/(mm·min^{-1})	黏土重量/kg	位移/mm	剪切力/kN	含水率/%
5	19.62	50	0.84	23.5
	19.52		0.93	22.0
	19.54		1.27	21.0
	19.59		1.40	20.5
	19.62		1.55	19.0
10	19.66	50	0.56	23.5
	19.64		0.96	21.5
	19.54		1.32	20.5
	19.59		1.48	20.0
	19.58		1.68	19.5
20	19.65	50	1.16	23.0
	19.53		1.26	22.0
	19.59		1.32	21.5
	19.61		1.49	21.0
	19.58		1.84	20.5

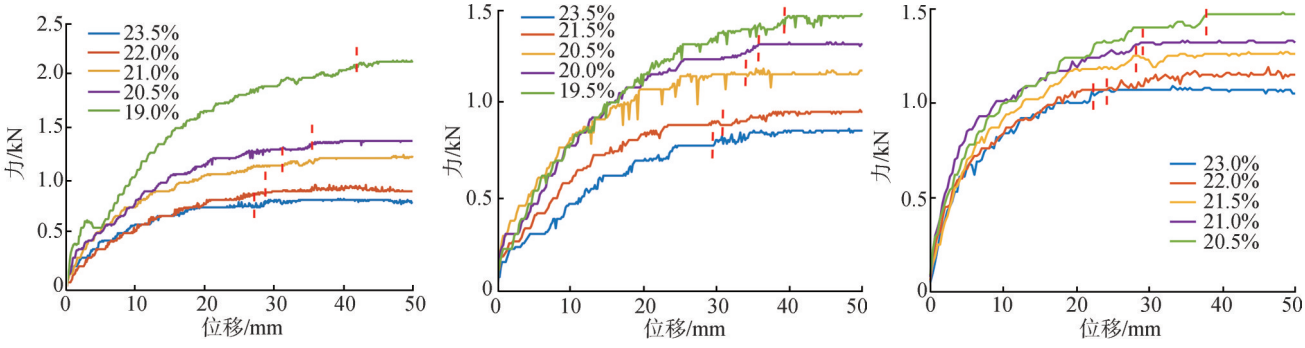

(a) 5 mm/min (b) 10 mm/min (c) 20 mm/min

图3 不同加载速率下含水率与加载曲线关系

Fig. 3 Relationship between water content and loading curves under different loading rates

2.2 振铃计数规律分析

振铃计数是指AE信号越过阈值的振荡次数。为了探究不同加载速率、不同含水率下振铃计数的变化规律，计算15组试验的振铃计数强度（即加载期间每单位时间振铃计数的平均值，以下取3 s为单位时间），并映射为圆的面积作图，不同加载速率及含水率下的振铃计数如图4所示。由图4（a）可知，在相同加载速率下，含水率越低，AE信号活动性越强烈，振铃计数强度越大。如：在5 mm/min加载速率下单位时间振铃计数分别为501、2 461、6 245、9 330、16 234；含水率降低增加了黏土稠度，使土体变硬，回填材料在周围较硬土体的压迫下产生更强的摩擦甚至破碎，使振铃计数

强度明显增加。此外,加载速率与振铃计数强度有一定的正相关性,较高加载速率下的振铃计数强度更大。

由图 4(b)~(d)可知,随着加载时间的增加,振铃计数强度也不断增加。其原因是试验初期土体正处于一个压密阶段,声发射事件数较少,随着剪切位移增大,土体颗粒开始挤压、摩擦甚至破坏,并以弹性波的形式对外释放能量,AE 事件数明显增多,幅值也在增大,这表明土体的变形和破坏程度在不断加剧。

为进一步研究振铃计数随含水率变化的趋势,将不同加载速率下的振铃计数进行分布拟合,如图 5 所示。由图 5 可知,振铃计数强度随着含水率的增加呈幂函数减小,能够在一定程度上揭示土体含水量或稠度的变化。

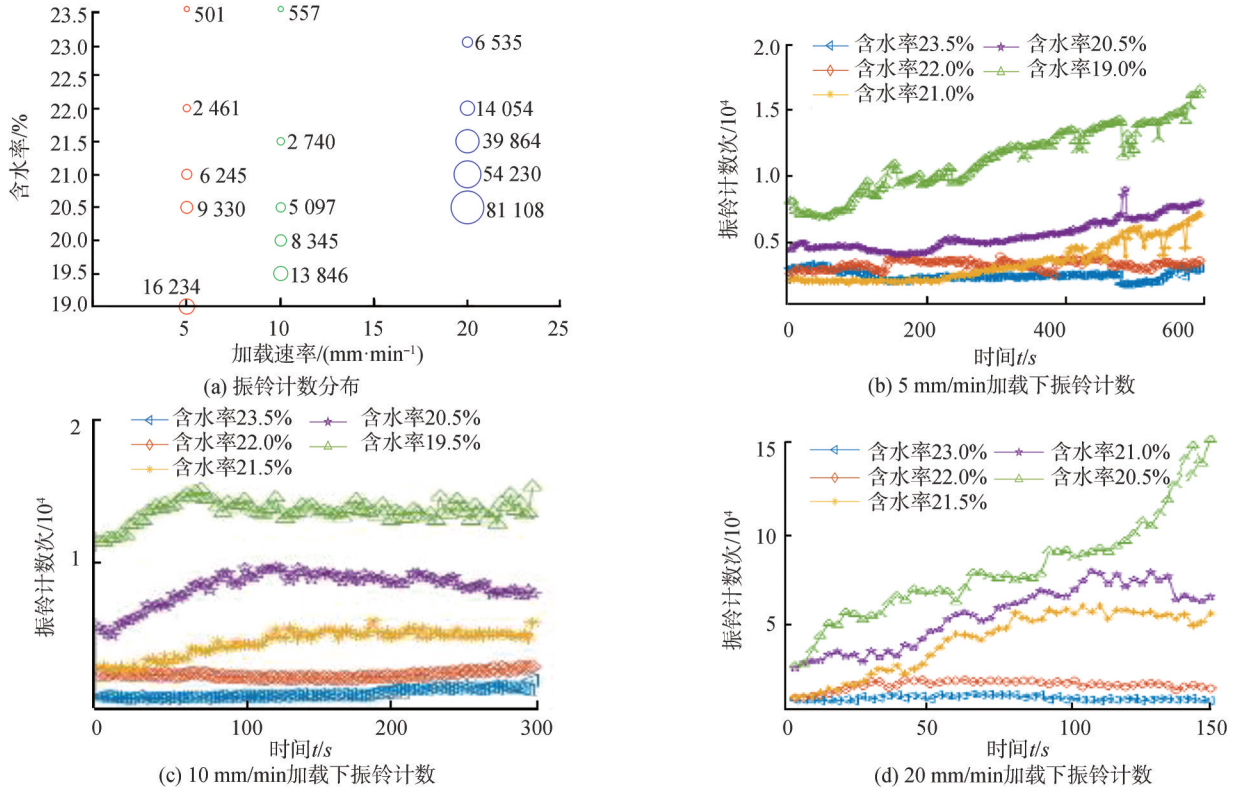

图 4　不同加载速率及含水率下的振铃计数

Fig. 4　Ringing counts under different loading rates and moisture contents

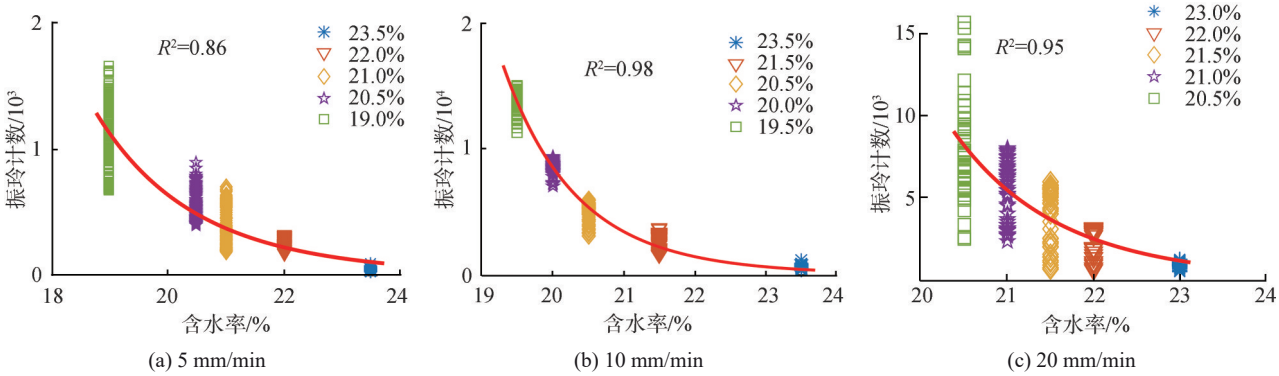

图 5　不同加载速率下振铃计数拟合曲线

Fig. 5　Fitting curves of ring counts under different loading rates

2.3　能量规律分析

不同加载速率及含水率下的声发射能量如图 6 所示。声发射能量是信号检波包络线下的面积,不同加载条件下的分布规律如图 6(a)所示,利用 3 s 为单位时间计算 AE 能量均值并用圆形面积表示。显然,相同加载速率下,能量随含水率降低而逐渐增大,如 5 mm/min 加载下,含水率为 23.5%、22.0%、21.0%、20.5%、19.0%的黏土体平均释放能量分别为 56 440、65 561、70 503、769 14 和 82 082 ms·mV,其他两组不同加载速率试验结果均表现出很好的一致性。由于含水率升高,土体

稠度会降低，有源波导系统整体刚度降低，填充材料之间的作用力容易通过土体塑性变形得以释放，因此声发射信号能量就会逐渐减小。此外，近似含水率条件下，能量会随加载速率的升高而增大。

由图 6(b)~(d)可知，能量随时间变化相对不大，呈缓慢变化或近似平稳。

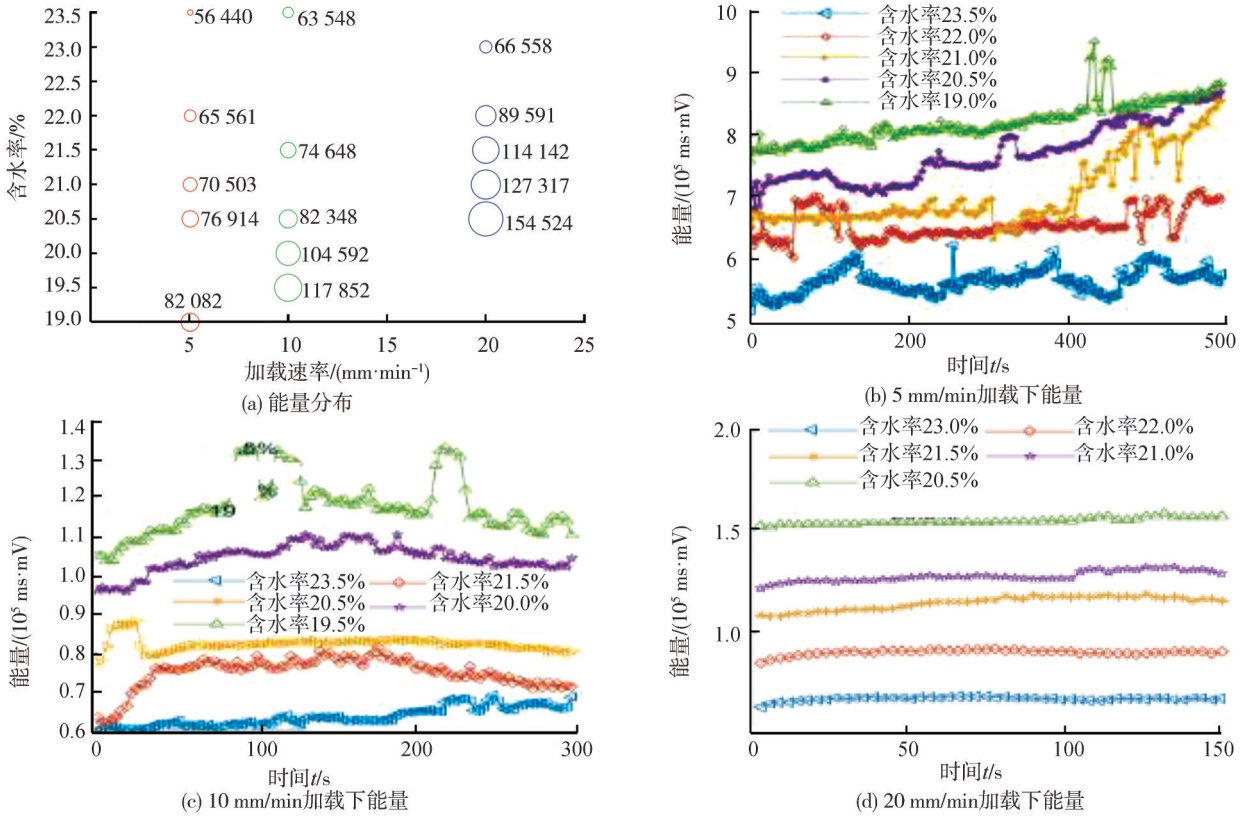

图 6　不同加载速率及含水率下的声发射能量

Fig.6　Energy at different loading rates and moisture contents

2.4　*b* 值规律分析

b 值是声发射试验中的一个重要参数，是象征剪切破裂的重要前兆之一。一般而言，*b* 值越小说明高幅值事件所占比例越大，采用最大似然法计算声发射 *b* 的值[27-28]：

$$b=\frac{20\lg \mathrm{e}}{A-A_{\min}} \qquad (1)$$

式中，A 为平均幅值，$A_{\min}$ 为最小幅值，e 为自然常数。

测试结果 *b* 值变化曲线如图 7 所示。由图 7 可知：当剪切速率为 5 mm/min 时，含水量为 23.5% 的 *b* 值减小趋势明显，其余 4 条缓慢降低或总体趋势平稳；剪切速率为 10、20 mm/min 时，*b* 值变化规律较为明显，总体上都随剪切位移增大而逐渐减小，到一定程度后基本保持稳定，表明剪切位移增加导致破坏能量释放不断加大，高幅值事件占比也逐渐增大，且在宏观破裂发生后 *b* 值基本保持稳定。

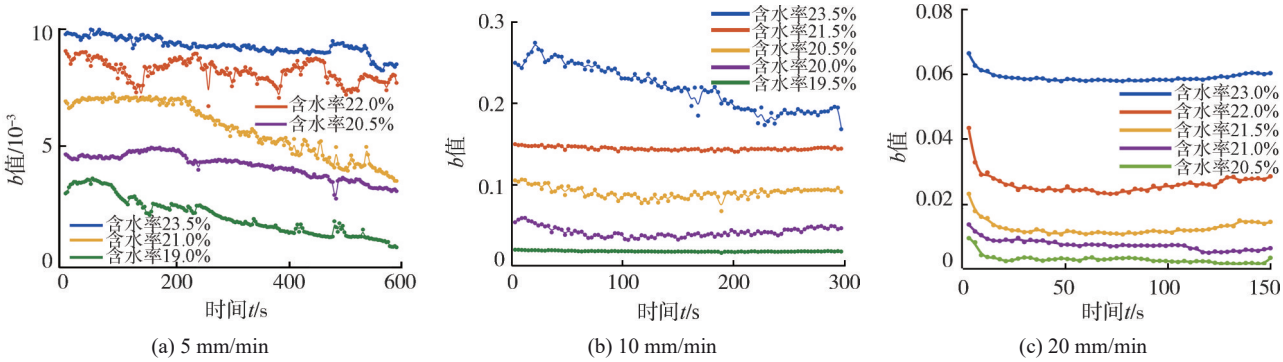

图 7　不同加载速率下含水率与 *b* 值关系

Fig.7　Relationship between moisture contents and *b*–values under different loading rates

含水量对b值的影响同样明显。不同加载速率下b值拟合曲线如图8所示。在剪切速率不变的情况下,随含水量增加b值也不断增加。原因是含水量增加后弱结合水增多,其充当了滑动水膜层,降低了剪切过程中固体团粒的机械挤压、摩擦或破碎作用,因此b值变大。拟合结果表明,随着含水率的升高,b值近似呈幂函数增加。

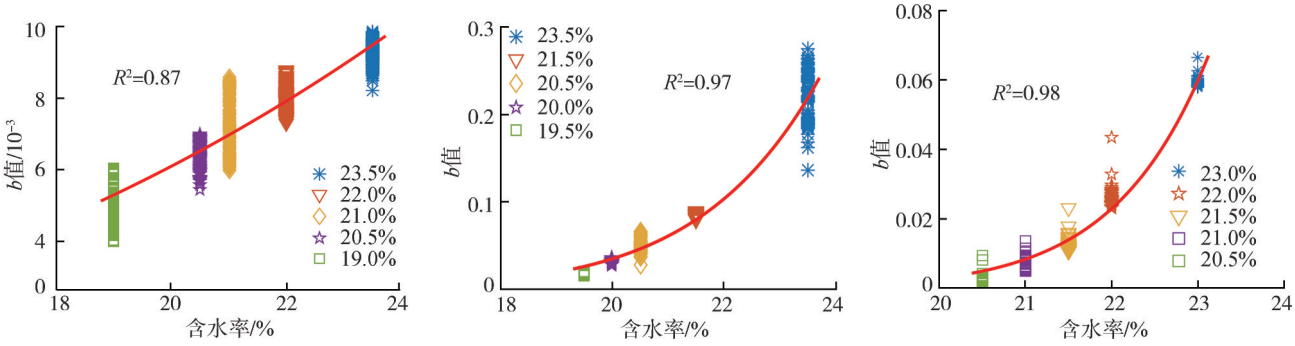

(a) 5 mm/min　　(b) 10 mm/min　　(c) 20 mm/min

图8　不同加载速率下b值拟合曲线

Fig.8　Fitting curves of b–values under different loading rates

2.5　特征参数聚类特性

AE特征参数模式识别如图9所示。不同加载速率及含水率下,土体剪切过程AE信号特征可能还涉及多因素演化过程,利用聚类分析进一步揭示相关多因素分类模式识别问题。3种不同加载速率下振铃计数与b值的关系分别如图9(a)、(c)、(e)所示。由图9可知,振铃计数与b值呈负相关,即振铃计数越大b值越小,加载速率为5、10、20 mm/min时的拟合曲线R^2分别为0.98、0.98、0.90,总体相关性高,且较低加载速率下数据拟合度更好。

含水率对振铃计数–b值特征空间数据分布也有明显影响。含水率较高时,试验结果分布于该空间左上角,具有较高的b值和较低的振铃计数;随含水率的降低,特征向量逐次向该空间右下方移动,且具有很好的规律性,即低含水率试样AE特征总是具有更低的b值和更大的振铃计数。

为探索各参数在特征空间中的可聚类性,可从紧致性、分离性和重叠度等方面对聚类结果进行评估[29]。因此,将主要利用类间分离度(class separation)和重叠区域比例(overlap ratio)两个指标进行分析。类别中心坐标:

$$(A_{ix},A_{iy})=\left(\frac{1}{T_i}\sum_{i=1}^{T_i}I_{ix},\frac{1}{T_i}\sum_{i=1}^{T_i}I_{iy}\right) \tag{2}$$

式中,A_{ix}、A_{iy}分别为第i种含水率类别中心的横、纵坐标,I_{ix}、I_{iy}分别为第i种含水率下各样本点的横、纵坐标(即每秒的振铃计数和能量),T_i为第i种含水率样本点的总数。

类间距离为:

$$M_{ij}=\left(\left(A_{ix}-A_{jx}\right)^2+\left(A_{iy}-A_{jy}\right)^2\right)^{\frac{1}{2}} \tag{3}$$

式中,A_{jx}、A_{jy}分别为第j簇含水率类别中心的横、纵坐标。

类内距离为:

$$S_i=\frac{\sum_{i=1}^{T_i}\left(\left(I_x-A_{ix}\right)^2+\left(I_y-A_{iy}\right)^2\right)^{\frac{1}{2}}}{T_i} \tag{4}$$

式中,I_x、I_y分别为第i种含水率类别各样本点的横、纵坐标。

因此,类间分离度为:

$$C=\sum_{i,j=1}^{K}M_{ij}\Big/\sum_{i=1}^{K}S_i,\ i\neq j \tag{5}$$

式中,K为含水率的类别数。

由于不同类别的样本有可能位于特征空间的重叠区域,即重叠样本,在多维空间中类重叠区域Ω可描述为:至少存在2个不同类别C_a和C_b同时表现出大于0的概率密度的区域[30]。为表征样本数据中各类别之间的区分度,引入重叠区域比例代表各个类别的区分程度,数据集的重叠区域比例是指重叠区域面积相对于总数据面积的比值,可表示为:

$$O=\sum_{i=1}^{P}S_{\Omega i}\Big/\sum_{i=1}^{C}S_{Ci} \tag{6}$$

式中,$S_{\Omega i}$、S_{Ci}分别为重叠区域和类别的面积,P为重叠区域的个数,C为类别的个数。

相关分析结果如图9(b)、(d)、(f)所示,能量与振铃计数成正相关。含水率对振铃计数–能量空间中数据的分布影响是明显的,较高含水率总是分布于左下

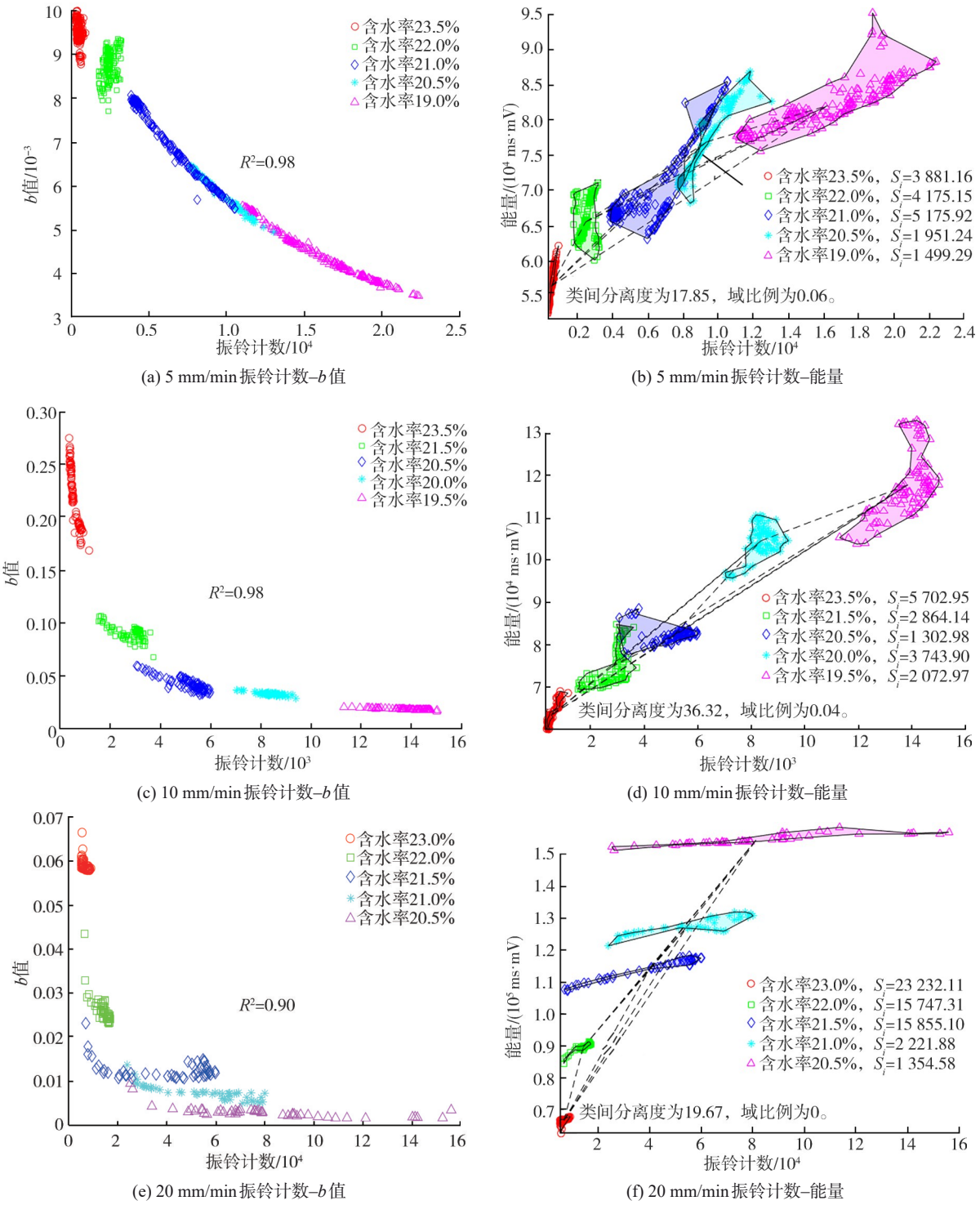

图9 AE特征参数模式识别

Fig.9 AE feature parameter pattern recognition

角，即更小的能量和振铃计数，而增加含水率后试验结果分布逐次向右上角移动，即能量和振铃计数同时增大。加载速率对其分布形态亦有一定影响，较高剪切速率下（如20 mm/min）其数据分布更为扁长。

类间分离度是所有类别内部样本点到类别中心的平均距离和与不同类别类别中心之间的距离和之比，其值越大则表示分类效果越明显。由图9（b）、（d）、（f）可知，重叠区域比例分别为0.06、0.04和0，各样本在该特征空间中均展示出分离度较高、重叠面积低的特点，尤其是高剪切速率下重叠区域比例更少。

由此可见，土体剪切过程AE信号特征伴随着多因素演化过程，通过多因素分类及模式识别等进行辨

识,可为声发射在土质边坡滑动预测预警的多特征参数选取提供理论依据。

3　结　论

基于有源波导杆系统的土体双面剪切试验过程AE信号特征参数分析,揭示了振铃计数、能量及*b*值等随剪切速率和含水率演化规律,以及多因素演化过程,研究可为声发射监测在土质边坡滑动预测预警的特征指标选取提供理论依据。

1)随着剪切位移增加,振铃计数迅速增大,且含水率越小,振铃计数强度越大;振铃计数强度随着含水率的增加呈幂函数减小,即振铃计数能很好地描述土体剪切过程含水量或稠度的变化,具有明显规律性和一致性。

2)在土体剪切位移过程中,能量呈现相对平稳或缓慢增加趋势,而土体含水率对能量影响很大,含水率越低其AE能量越大;此外,在近似含水率条件下,加载速率越大其能量亦越大。

3)*b*值随着剪切位移增加先降低后平缓,直到宏观破裂发生后,*b*值基本稳定;含水率越大,*b*值则越大,主要原因在于弱结合水膜充当的滑动层减少了剪切过程的能量释放。

4)基于有源波导杆系统的土体双面剪切试验过程AE信号总是伴随着多因素演化过程,通过多因素分类及模式识别等进行辨识,可为声发射在土质边坡滑动预测预警的多参数指标选取提供依据。

参考文献:

[1] Yin Yueping,Cheng Yuliang,Liang Jingtao,et al.Heavy-rainfall-induced catastrophic rockslide-debris flow at Sanxicun, Dujiangyan,after the Wenchuan Ms 8.0 earthquake[J].Landslides,2016,13(1):9–23.

[2] Xu Chong, Tian Yingying, Zhou Bengang, et al. Landslide damage along Araniko highway and Pasang Lhamu highway and regional assessment of landslide hazard related to the Gorkha,Nepal earthquake of 25 April 2015[J].Geoenvironmental Disasters,2017,4(1):14.

[3] Li Hongying,Tan Yuehu,Li Erbing.Sensitive factors analysis of stability of Tiansan landslide at carla hydropower station[J]. Journal of Hohai University(Natural Sciences), 2012,40(4):420–425.[李红英,谭跃虎,李二兵.卡拉水电站田三滑坡体稳定性敏感因素分析[J].河海大学学报(自然科学版),2012,40(4):420–425.]

[4] Wu Shuren, Wang Tao, Shi Jusong, et al. A review of engineering landslide prevention and control[J]. Geological Bulletin of China,2013,32(12):1871–1880.[吴树仁,王涛,石菊松,等.工程滑坡防治关键问题初论[J].地质通报,2013,32(12):1871–1880.]

[5] Uhlemann S,Smith A,Chambers J,et al.Assessment of ground-based monitoring techniques applied to landslide investigations[J].Geomorphology,2016,253:438–451.

[6] Hu Wei, Li Shulin. A study on the acoustic emission technology in the analysis of rock slope stability[J].Mining Research and Development,2002,22(3):9–11.[胡伟,李庶林.岩质边坡稳定性分析中的AE技术研究[J].矿业研究与开发,2002,22(3):9–11.]

[7] Yi Wu, Meng Zhaoping. Study on acoustic emission feature of rock slope and its instability forecast criterion[J]. Rock and Soil Mechanics,2007,28(12):2529–2533.[易武,孟召平.岩质边坡声发射特征及失稳预报判据研究[J].岩土力学,2007,28(12):2529–2533.]

[8] Smith A, Dixon N. Acoustic emission behaviour of dense sands[J].Géotechnique,2019,69(12):1107–1122.

[9] Shiotani T.Evaluation of long-term stability for rock slope by means of acoustic emission technique[J].NDT & E International,2006,39(3):217–228.

[10] Dixon N, Spriggs M. Quantification of slope displacement rates using acoustic emission monitoring[J].Canadian Geotechnical Journal,2007,44(8):966–976.

[11] Li Gang. Simulation experimental study on acoustic emission characteristics of slope failure monitoring based on waveguide rod[D]. Ganzhou: Jiangxi University of Science and Technology,2017.[李刚.基于波导杆监测边坡破坏的声发射特性模拟试验研究[D].赣州:江西理工大学,2017.]

[12] Li Wenbiao, Wang Yi, Chen Xin, et al. Fractal analysis of similar simulation of embankment failure process based on acoustic emission monitoring technology[J]. Highway, 2017,62(7):33–38.[李文彪,王轶,陈新,等.基于声发射监测的路堤相似模拟破坏过程分形特征研究[J].公路,2017,62(7):33–38.]

[13] Codeglia D,Dixon N,Fowmes G J,et al.Analysis of acoustic emission patterns for monitoring of rock slope deformation mechanisms[J].Engineering Geology,2017,219:21–31.

[14] Jiang Yao,Wang Gonghui,Kamai T.Acoustic emission signature of mechanical failure:Insights from ring-shear friction experiments on granular materials[J].Geophysical Research Letters,2017,44(6):2782–2791.

[15] Hu Wei,Scaringi G,Xu Qiang,et al.Acoustic emissions and microseismicity in granular slopes prior to failure and flow-like motion: The potential for early warning[J]. Geophysical Research Letters,2018,45(19):10406.

[16] Berg N, Smith A, Russell S, et al. Correlation of acoustic emissions with patterns of movement in an extremely slow-moving landslide at Peace River, Alberta, Canada[J]. Canadian Geotechnical Journal,2018,55(10):1475–1488.

[17] Michlmayr G, Cohen D, Or D. Sources and characteristics

of acoustic emissions from mechanically stressed geologic granular media—A review[J]. Earth-Science Reviews, 2012, 112(3/4):97–114.

[18] Dixon N,Hill R,Kavanagh J.Acoustic emission monitoring of slope instability: Development of an active waveguide system[J].Proceedings of the Institution of Civil Engineers–Geotechnical Engineering,2003,156(2):83–95.

[19] Dixon N, Smith A, Flint J A, et al. An acoustic emission landslide early warning system for communities in low-income and middle-income countries[J]. Landslides, 2018, 15(8): 1631–1644.

[20] Dixon N,Spriggs M P,Smith A,et al.Quantification of reactivated landslide behaviour using acoustic emission monitoring[J].Landslides,2015,12(3):549–560.

[21] Smith A,Dixon N,Meldrum P,et al.Acoustic emission monitoring of a soil slope:Comparisons with continuous deformation measurements[J]. Géotechnique Letters, 2014, 4(4): 255–261.

[22] Koerner R M,McCabe W M,Lord A E.Acoustic emission monitoring of soil stability[J].Journal of the Geotechnical Engineering Division,1978,104(5):571–582.

[23] Lord A E,Fisk C L,Koerner R M.Utilization of steel roads as AE waveguides[J].Journal of the Geotechnical Engineering Division,1982,108(2):300–305.

[24] Voight B.A relation to describe rate-dependent material failure[J].Science,1989,243(4888):200–203.

[25] Spriggs M P.Quantification of acoustic emission from soils for predicting landslide failure[D]. Loughborough: Loughborough University,2005.

[26] Smith A,Heather–Smith H J,Dixon N,et al.Acoustic emission generated by granular soil-steel structure interaction [J].Géotechnique Letters,2020,10(2):119–127.

[27] Wu Xin,Wang Xuemei,Luo Xiaoyu,et al.Analysis of three-point bending acoustic emission parameters of wave guide rod under different loading rates[J]. China Safety Science Journal,2021,31(10):159–166.[吴鑫,王雪梅,罗筱毓,等.不同加载速率下波导杆三点弯曲声发射参数分析[J].中国安全科学学报,2021,31(10):159–166.]

[28] Zhao Hongxia, Wu Xin, Luo Xiaoyu, et al. Experimental study on characteristics of acoustic emission signals induced by seepage process of tailings sand medium[J].Journal of Safety Science and Technology,2021,17(9):97–102.[赵红霞,吴鑫,罗筱毓,等.尾矿砂介质渗流过程诱发声发射信号特征试验研究[J].中国安全生产科学技术,2021,17(9):97–102.]

[29] Tang Yiming,Pan Zhifu,Pedrycz W,et al.Viewpoint-based kernel fuzzy clustering with weight information granules [J].IEEE Transactions on Emerging Topics in Computational Intelligence,2023,7(2):342–356.

[30] Ozkan I,Türkşen I B.MiniMax ε-stable cluster validity index for Type–2 fuzziness[J].Information Sciences,2012,184 (1):64–74.

Evolution of Acoustic Emission Characteristics During Soil Shear Testing Based on Active Waveguide System

WU Xin[1,2], *LIU Yonghong*[1], *WANG Xuemei*[1,3], *ZHANG Man*[1]

(1.College of Engineering, Sichuan Normal University, Chengdu 610101, China;
2.Key Laboratory of Land Resources Evaluation and Monitoring in Southwest, Ministry of Education, Sichuan Normal University, Chengdu 610068, China;
3.Meishan City Emergency Management Bureau, Meishan 620020, China)

Abstract:

Objective Monitoring internal shear processes and assessing potential risk perception in landslides is crucial for maintaining the stability of earthy slopes. This research uses an active waveguide system and acoustic emission (AE) technology to examine the evolution of AE signal characteristics under different shear conditions. The primary objectives are to 1) characterize the behavior of AE signals, including ring count, energy, and *b*–value, during the soil shear process, 2) analyze the influence of water content and loading rate on AE signal evolution, as these factors significantly affect soil stability, 3) establish a theoretical framework for selecting characteristic indicators that enhance the predictive capabilities of AE technology in monitoring soil slope stability, 4) support the development of more effective monitoring and early warning systems for soil slope sliding, improving the safety and management of infrastructure and human settlements in landslide-prone areas.

Methods Through a systematic experimental approach, the study aimed to uncover the multifactorial dynamics of AE signals during soil shear, providing valuable insights for the application of AE technology in geotechnical engineering and slope stability assessments. The research methodology was designed to systematically investigate the AE characteristics of soil under shear conditions using an active waveguide system. The approach encompassed several key stages, beginning with the selection and preparation of the soil material. Chengdu clay, representative of high-water-content soils, was chosen for its prevalent geotechnical properties, including high water content and a complex pore structure. The clay was meticulously compacted within a specially designed shear box, ensuring a controlled environment for the experiments. An active waveguide rod was integrated into the setup to enhance the sensitivity of AE signal detection and reduce signal attenuation, a common challenge in granular me-

dia. The waveguide rod was positioned within a granular material bed, facilitating the transmission of AE signals from the shear zone to the sensors. The experimental design involved varying two critical parameters: the loading rate and the water content of the soil. Three distinct loading rates (5, 10, and 20 mm/min) and five different water content levels were selected, resulting in a comprehensive matrix of 15 test conditions. Each test was conducted under displacement control, with a predetermined shear displacement of 50 mm, beyond which the test was halted to analyze the accumulated AE data. The AE signals were captured using a DS5–16 *b*–type data acquisition system with a sampling frequency of 3 MHz and a frequency response range of 100 to 400 kHz. The system recorded the AE events, including the ring count, energy, and *b*–value, which were essential parameters for analyzing the soil's shear behavior. The data collected were then subjected to statistical and cluster analyses to identify the underlying patterns and correlations between the AE parameters and the experimental conditions. This comprehensive methodology established a robust understanding of the AE signal evolution during soil shear, providing insights into the multifactorial processes involved and contributing to the development of predictive models for soil slope stability.

Results and Discussions The research yielded substantial insights into the behavior of AE signals during the shear testing of soil, underpinned by the analysis of three pivotal AE parameters, ring count, energy, and *b*–value, each responding distinctly to variations in shear displacement and soil water content. Ring count findings: The research identified that the ring count escalates swiftly with an increase in shear displacement, with drier soils demonstrating heightened AE signal activity. This indicates that soil moisture plays a critical role in the generation of AE signals. The ring count's exponential decline with increasing water content highlights the need to consider soil consistency in AE monitoring systems. Energy observations: The study demonstrated that AE energy, representing the aggregate energy emitted during soil shearing, exhibits a gradual increase with shear displacement. Soils with reduced water content were observed to release higher energy, likely due to greater frictional resistance in less hydrated conditions. In addition, the energy output was shown to escalate with faster loading rates, indicating the importance of the rate of stress application in energy release. *b*–value insights: The *b*–value, a measure of AE event magnitude distribution, displayed a trend of decreasing initially with shear displacement and then leveling off. This trend implies that as soil approaches failure, there is a rise in the proportion of high-magnitude AE events. The *b*–value is negatively correlated with water content, with higher water content of soil showing larger *b*–values, potentially attributable to the water's lubricating effect, which can decrease frictional energy dissipation. Multifactorial Analysis: Cluster analysis clarified the multifactorial nature of AE signal characteristics influenced by shear rate and water content. The analysis showed distinct patterns between different water content groups, with lower water content correlating with lower *b*–values and higher ring counts. In addition, a positive correlation was observed between energy and ring count, with both parameters increasing with water content. The impact of the loading rate on result distribution was also noted, with higher shear rates leading to more pronounced class separation.

Conclusions This study concludes that AE signal characteristics are sensitive indicators of soil behavior during shear, demonstrating significant potential to enhance the predictive capabilities of AE technology in soil slope stability monitoring. The findings highlight the necessity of a detailed understanding of the interaction between AE parameters and soil properties, which is essential for developing accurate monitoring systems. It highlights the value of employing a multi-parameter analysis in AE-based monitoring to achieve a more comprehensive evaluation of soil slope conditions. The study advances the development of early warning systems capable of detecting the onset of slope instability with increased precision by integrating insights from ring count, energy, and *b*–value analyses. These conclusions affirm the effectiveness of AE technology in geotechnical engineering, particularly for predicting and alerting against soil slope failure. The results provide a theoretical foundation for applying AE in monitoring, providing a basis for future research and practical applications in soil mechanics and slope stability management.

Key words: soil shear; loading rate; moisture content; acoustic emission; characteristic parameters

（编辑　周　璇）

引用格式: Wu Xin,Liu Yonghong,Wang Xuemei,et al.Evolution of acoustic emission characteristics during soil shear testing based on active waveguide system[J].Advanced Engineering Sciences,2025,57(3):96–105.[吴鑫,刘永红,王雪梅,等.基于有源波导系统土体剪切试验过程声发射特征演化规律[J].工程科学与技术,2025,57(3):96–105.]